TOWARD AUTOMATIC ZONAL SEGMENTATION OF PROSTATE BY COMBINING A DEFORMABLE MODEL AND A PROBABILISTIC FRAMEWORK

Makni N.[1,2] , Puech P.[1,3], Lopes R.[1,2], Dewalle A.S.[1], Colot O.[2], Betrouni N.[1], Member, IEEE

[1] Inserm, U703, ITM, Pavillon Vancostenobel, CHRU Lille, 59037, France

[2] LAGIS CNRS UMR 8146, USTL, Villeneuve d'Ascq, 59655, France

[3] Radiology Department, University Hospital, Lille, France

ABSTRACT

This paper introduces an original method for automatic 3D segmentation of the prostate gland from Magnetic Resonance Imaging data. A statistical geometric model is used as *a priori* knowledge. Prostate boundaries are then optimized by a Bayesian classification based on Markov fields modelling. We compared the accuracy of this algorithm, free from any manual correction, with contours outlined by an expert radiologist. In 3 random cases, including prostates with cancer and benign prostatic hypertrophy (BPH), mean Hausdorff's distance (HD) and Overlap Ration (OR) were 8.07 mm and 0.82, respectively. Despite fast computing times, this new method showed satisfying results, even at prostate base and apex. Also, we believe that this approach may allow delineating the peripheral zone (PZ) and the transition zone (TZ) within the gland in a near future.

Key Words **—** Prostate cancer, segmentation, 3D deformable model, Markov fields.

1. INTRODUCTION

In the last decade, Magnetic Resonance Imaging (MRI) has been a reference for assessment of prostate cancer extension. It has been carried out only when the tumor has already been diagnosed by means of biopsies. Prostate segmentation applications used for real-time interventional procedures are usually based on Ultrasound imaging (US) [1]. Nevertheless, there is a recent interest in imaging for treatment planning of robotized surgery or emerging focal cancer ablation techniques (HIFU, photodynamic or thermal therapy,…). In these cases, MRI is best suited because it provides a better contrast resolution for tissue characterization and allows full 3D description of the gland, potential regions of interest, and surrounding structures. In the field of prostate segmentation, various image processing techniques have been investigated : Mazonakis *and al.* [2] presented a CT-based growing region-based technique for prostate, bladder and rectum segmentation, in which user intervention remained necessary for thresholds definition. Freedman *and al.* [3] combined an appearance and form model with probability distribution of object-inside photometric variables for prostate and rectum segmentation. As far, Pasquier *and al.* [4] presented a deformable model-based method for automatic volume definition in conformal radiotherapy planning. A manual correction was necessary for both apex and base of the gland where the contrast between prostate and surrounding structures (muscles and seminal vesicles, respectively) is a challenging issue. In this paper, we refine these results using a Markov fields-based Bayesian framework.

2. METHOD

We consider 2 random fields $X = \{x_s , s \in S\}$ and $Y = \{y_s , s \in S\}$, where S is the set of voxels. Each x_s takes its values in a finite set of labels $\Omega=\{-1, 1\}$ and each y_s takes its value in the set of the MR image grey levels.

The approach described in this paper is a Bayesian segmentation that can be summarized in four steps:

i) Integration of prostate 3D model, that will be used as an initial labelling X°.

ii) Characterization of an *a priori* probability P(X) of voxels' labelling, using Markov field modelling.

iii) Establishment of a conditional law for the image grey levels P (Y | X).

iv) Estimation of the optimum labels field X, that maximizes the *a posteriori* probability P(X|Y).

Figure 1 shows the organizational structure of the method.

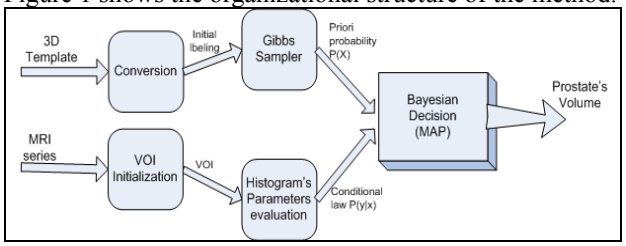

Figure 1 - Global scheme of the method

2.1. 3D Model

In a previous work [4;5], a generic prostate model had been established from a training base of 20 manual outlines. The model, deduced by a principal component analysis, is composed of an average shape and of the most important deformation directions. The model is initialized on the image, and a heuristic optimization by the simulated annealing algorithm is performed to estimate the best parameters describing the prostate's contours. This first 3D contour is converted into a set of labels by attributing +1 to voxels that belong to prostate and -1 to those that do not. Consequently, an initial labels' vector X° is established.

2.2. *A priori* probability

The initial labelling X° cannot be operated without ensuring that it performs a Markov field. Precisely, according to Hammersley-Clifford's theorem (1971) for which a demonstration is given in [6], X is a Markov field if and only if it follows a Gibbs' distribution, defined as follows:

$$P(x) = \frac{1}{Z}\exp[-U(x)] \quad (1)$$

$$U(x) = \sum_{c\in C} J_c(x) \quad (2)$$

Where J_c is a clique-related potential that will be defined further on, X_c is the restriction on the clique c, and C is the set of S cliques.

To meet this requirement, we use the Gibbs' sampler algorithm. Frequently cited in the literature [7], it can generate a Markov field from any vector of labels. In order to do that, we have to express the *a priori* probability P(X), thus defining the energy function U(x). We will then use Potts' (or Ising) model [8;8] which defines U(x) as :

$$U(x) = -\beta\sum_{s\in S} x_s - \alpha\sum_{s\in S} x_s\Big(\sum_{t\in V_s} x_t\Big) \quad (3)$$

Evaluation of parameters α and β is usually carried out by estimation methods and fairly generic approximations [6]. In this work, we decided to determine them through simulation, as we have sufficient information about the X field. We consider a 26-connexity system, in which the labels' sum in each voxel's neighbourhood takes a value ranging [-27, 27]. Figure 2 shows the variation of $P(x_s=1|x_{V_s})$ for different values of α and β=0 :

$$P(x_s = 1 \mid x_{Vs}) = \frac{\exp[-U(1, x_{Vs})]}{\sum_{k\in\Omega}\exp[-U(k, x_{Vs})]} = \frac{\exp[\alpha.\sum_{t\in Vs} x_t]}{\sum_{k\in\{-1;1\}}\exp[\alpha.k.\sum_{t\in Vs} x_t]} \quad (4)$$

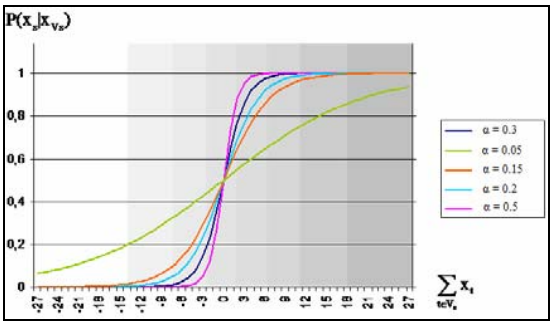

Figure 2 - *A priori* probability simulation

From simulation results we can establish that $P(x_s = 1 \mid x_{Vs})$ is "blurred" when α decreases; assigning a tiny value to α (0.15 or 0.05) allows having a less deterministic labelling, which authorizes further evolution possibilities. We set α to 0.15 and, by a similar simulation, β is set to 0.

2.3. Image formation law

In order to model P(Y|X), the conditional probability of image values knowing the labels field, we conducted a statistical study on gray levels. After processing the histogram in a Volume Of Interest (VOI), we could approximate it by a mixture of Gaussians, which parameters (μ_i, σ_i, k_i) would be automatically extracted using a mode recognition algorithm [9]. Gray levels' histogram mainly contains three modes:

i) The first mode, which mean is located in the black levels, represents tissues and fat surrounding the prostate. In our study, we make it correspond to the -1 class.

ii) The second mode is the largest one: it represents the gray levels of prostate's transition zone.

iii) The last mode is situated in the high gray levels, and despite its small size, has an important significance: it represents tissue of prostate's peripheral zone, and eventually some cysts in the transition zone.

We can then approximate the conditional probability of a voxel's gray level knowing its label by:

$$P(y_s \mid x_s = \omega) = \frac{1}{Z_y}.\frac{1}{\sqrt{2\pi}\sigma_\omega}\exp[-\frac{1}{2}(\frac{y_s-\mu_\omega}{\sigma_\omega})^2] \quad (5)$$

where Z_y is a normalization constant, and (μ_ω, σ_ω) are Gauss parameters of class ω. As a first approach, this expression faces an ambiguity as two Gaussian modes could both be representative of prostate. We solve this problem by comparing distances between voxel's gray level y_s and each mode's mean μ_i.

$$P(y_s \mid x_s = 1) = \frac{1}{Z_y}.\frac{1}{\sqrt{2\pi}\sigma_i}\exp[-\frac{1}{2}(\frac{y_s-\mu_i}{\sigma_i})^2] \quad (6)$$

where $i=\arg[\min(\frac{y_s-\mu_i}{\sigma_i})^2]$.

Finally, we model the image formation law as follows:

$$P(y_s \mid x_s = \omega) = \begin{cases} \frac{1}{Z_y}.\frac{1}{\sqrt{2\pi}\sigma_\omega}\exp[-\frac{1}{2}(\frac{y_s-\mu_\omega}{\sigma_\omega})^2] \text{ if } \omega=-1 \\ \frac{1}{Z_y}.\frac{1}{\sqrt{2\pi}\sigma_i}\exp[-\frac{1}{2}(\frac{y_s-\mu_i}{\sigma_i})^2] \text{ if } \omega=+1 \end{cases} \quad (7)$$

Where $i=\arg[\min(\frac{y_s-\mu_i}{\sigma_i})^2]$.

Markovianity of (Y, X)

As we adopt Hidden Markov Field Model, we can stipulate that:

- H1: $P(y_s|x)=P(y_s|x_s) \quad \forall s \in S$
- H2 : $P(y|x)=\prod_{s\in S} P(y_s|x)$

Hence:

$$P(y \mid x) = \prod_{s\in S} P(y_s \mid x_s) = \frac{1}{(Z_y.\sqrt{2\pi})^{|S|}}.\frac{1}{\prod_{s\in S}\sigma_{\omega(x_s)}}.\exp[\sum_{s\in S}(\frac{y_s-\mu_{\omega(x_s)}}{\sigma_{\omega(x_s)}})^2] \quad (8)$$

Where $\omega(x_s)$ is the class of voxel s.

Supposing $\prod_{s\in S}\sigma_{\omega(x_s)}$ globally constant, we may express P(y|x) as:

$$P(y \mid x) = \frac{1}{Z_{yx}}\exp[-H(y,x)] \quad (9)$$

where Z_{yx} is a constant and $H(y,x)=-\sum_{s\in S}(\frac{y_s-\mu_{\omega(x_s)}}{\sigma_{\omega(x_s)}})^2$ is the energy function defined on S.

According to Hammersley – Clifford theorem [7], (Y, X) is a Markov field. This conclusion is going to be helpful in the following section.

2.4. Estimation, optimization and decision

Based on the Maximum *A Posteriori* (MAP) decision method, voxels classification would consist in searching a labelling x* that maximizes P(x|y):

$$x^* = \arg[\max_{x\in\Omega^{|S|}}(P(x \mid y))] \quad (10)$$

According to Bayes' formula:

$$P(x \mid y) = \frac{P(x,y)}{p(y)} = \frac{P(x).P(y \mid x)}{p(y)} \propto P(x).P(y \mid x) \quad (11)$$

From this, according to equations (1) and (8):

$$P(x \mid y) \propto \frac{1}{Z_x.Z_{yx}}\exp[-U(x)-H(y,x)] \quad (12)$$

Since it is almost impossible to compute all labelling probabilities, we will assess the MAP by the Iterated Conditional Mode (ICM) estimator [6]. This determinist algorithm requires a relevant initialization, and consists on retaining the class that maximizes the probability $P(x_s|y)$ for each voxel:

$$x^* = \arg[\max_{x\in\Omega^{|S|}}(P(x \mid y))] \Leftrightarrow \begin{cases} x^* = (x_s)_{s\in S} \text{ so that:} \\ \forall s \in S, x_s = \arg[\max_{x_s\in\Omega}(P(x_s \mid y))] \end{cases} \quad (13)$$

In addition, according to equation (11):

$$P(x_s|y) \propto P(x_s).P(y|x_s)$$

As (Y, X) and X are Markov fields, which globally means that probabilities are neighborhood-dependent, we are able to assume that:

$$P(x_s|y) \propto P(x_s).P(y|x_s) \propto P(x_s \mid x_{V_s}).P(y_s|x_s) \quad (14)$$

Hence, maximizing $P(x_s|y)$ could be done by maximizing $P(x_s \mid x_{Vs}).P(y_s \mid x_s)$. To do so, we implemented the ICM algorithm as follows:

- Initialize a first labelling map X°, using the Gibbs-sampled 3D model.
- *Repeat, for each iteration n:*
  - browse all sites and calculate for each the conditional probability $P_{n-1}(x_s|x_{Vs},y)$
  - apply the decision rule:
    $$x_s^n = \arg[\max_{x_s\in\Omega}(P(x_s|V_s,y))]$$
- *Until* reaching a little change between two successive iterations.

3. EXPERIMENTS AND RESULTS

The first tests were performed on T2-weighted BFFE images obtained on a Philips 1.5 T Achieva MRI device with a voxel size of 0.83 x 0.83 x 4 mm. Figure 3a illustrates results in a large prostate, showing BPH (112 cc), for which the deformable model alone was insufficient as prostate dimensions exceeded the generic model. Figure 3b shows a prostate with a large uniform low-intensity tumour of the right peripheral zone that mimics central zone signal, and could theoretically hinder automatic segmentation. Mean manual contouring time (MMCT) required for the expert radiologist on 15 slices was 18 min 20 sec [15-23 min.]. Mean automatic contouring time (MACT) required for our algorithm on a standard PC was 72 sec [64-83 sec.]. We compared the contours obtained with both methods (free from any manual correction) using Hausdorff's distances (HD) [10], Gravity Distance (GD), overlap ratios (OR), and Volume Properly Contoured (VPC). Results are detailed in table 1.

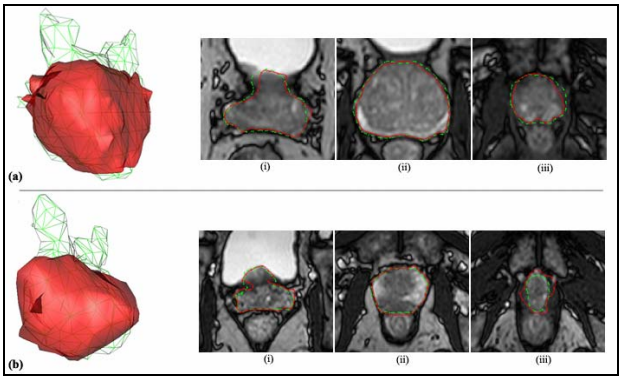

Figure 3 - Segmentation results presented at (i) base (ii) central zone (iii) apex and 3D visualisation. (a) Prostate with BPH. (b) prostate with a large low intensity tumour of PZ.

Patient	HD (mm)	GD (mm)	OR	VPC
1	7.24	2.97	0.81.	0.90
2	6.85	2.80	0.84	0.89
3	10.40	3.05	0.82	0.91
mean	**8.16**	**2.94**	**0.82**	**0.90**

Table 1 - Comparison of manual and automatic segmentation.

4. DISCUSSION AND CONCLUSION

In this study, we developed a method for automatic contouring of 3D prostate MRI that combines statistical information on prostate geometry, with a Bayesian segmentation based on Markov fields.

The first tests show that the integration of a Bayesian framework improves the results previously reported by [4] when using a deformable model alone, especially at the base and the apex, where surrounding tissues are in contact with the gland and hinder the deformable model. The well-known robustness of Markov models and rapid convergence of ICM estimator explain this increased performance. Nevertheless, minor contouring errors still persist at the apex, and our method still needs to be improved at this location. It should also be evaluated on a larger set of patients, and with different sequence parameters (thinner slices, higher spatial resolution) that may improve its accuracy.

This method was designed to be part of a multi-source prostate segmentation project, that will take account of other MRI sequences with different contrasts (T2-w, T1-w, diffusion-weighted,…). Data fusion based on Evidence theory could help resolve persistent issues at the apex. In addition, different settings of our method could be applied to distinguish transition from peripheral zone, which is an issue of major concern in clinical practice, especially for cancer treatment planning.

We plan to include this segmentation method in a prostate-dedicated computer aided diagnosis (CAD) software [11] designed for prostate cancer localization, volume assessment and treatment planning.

REFERENCES

[1] Fenster A, Surry K, Smith W, and B.Downey D, "The use of three-dimensional ultrasound imaging in breast biopsy and prostate therapy," Measurement, vol. 36, no. 3-4, pp. 245-256, 2004.

[2] M.Mazonakis, J.Damilakis, H.Varveris, P.Prassopoulos, and N.Gourtsoyiannis, "Image segmentation in treatment planning for prostate cancer using the region growing technique," Br J Radiol, vol. 74, pp. 243-248, 2001.

[3] D.Freedman, J.Radke Richard, Zhang Tao, J.Yongwon, M.Lovelock, and T.Y Chen George, "Model-based segmentation of medical imagery by matching distributions," IEEE Trans. Med. Img., vol. 24, no. 3, pp. 281-292, 2005.

[4] D.Pasquier, T.Lacornerie, M.Vermandel, J.Rousseau, E.Lartigau, and N.Betrouni, "Automatic segmentation of pelvic structures from MRI images for prostate cancer radiotherapy," Int J Radiation Oncology Biol. Phys., vol. 68, no. 2, pp. 592-600, Feb.2007.

[5] N. Betrouni, P. Puech, A. S. Dewalle, R. Lopes, P. Dubois, and M. Vermandel, "3D automatic segmentation and reconstruction of prostate on MR images," Conf. Proc. IEEE Eng Med. Biol. Soc., vol. 1, pp. 5259-5262, 2007.

[6] J.Besag, "Spatial interaction and the statistical analysis of lattice systems," Journal of Royal Statistical Society, vol. 36, pp. 192-236, 1974.

[7] Geman S and Geman D, "Stochastic relaxation, Gibbs distributions and the Bayesian restoration of images," IEEE Trans. on Pattern Analysis and MachineIntelligence, vol. 6, pp. 721-741, 1984.

[8] Potts R.B., "Some generalized order-disorder transitions," Proc. Camb. Phil. Soc., vol. 48, pp. 106-109, 1952.

[9] J.G.Postaire and C.Vasseur, "An approximate solution to normal mixture identification with application to unsupervised pattern classification," IEEE Trans. on Pattern Anal. & Machine Intelligence, vol. PAMI-3, no. 2, pp. 163-179, 1981.

[10] V.Chalana and Y.Kim, "A methodology for evaluation of boundary detection algorithms on medical images," IEEE Trans. Med. Imag, vol. 16, no. 5, pp. 642-652, 1997.

[11] P. Puech, N. Betrouni, R. Viard, A. Villers, X. Leroy, and L. L. Tre, "Prostate cancer computer-assisted diagnosis software using dynamic contrast-enhanced MRI," Conf. Proc. IEEE Eng Med. Biol. Soc., vol. 1, pp. 5567-5570, 2007.